Macromolecules
ARTICLE

Macromolecules **2009**, *42*, 5745–5751 **5745**
DOI: 10.1021/ma900973f

Interfacial Effects on Water Penetration into Ultrathin Ionomer Films: An in Situ Study Using Neutron Reflectometry

Lilin He,[†] Hillary L. Smith,[‡] Jaroslaw Majewski,[‡] Cy H. Fujimoto,[§] Christopher J. Cornelius,[§,⊥] and Dvora Perahia*[,†]

[†]*Department of Chemistry, Clemson University, Clemson, South Carolina 29634,* [‡]*Lujan Neutron Scattering Center, Los Alamos National Laboratory, Los Alamos, New Mexico 87545, and* [§]*Sandia National Laboratories, MS 0886, Albuquerque, New Mexico 87185-0886.* [⊥]*Current address: Department of Chemical Engineering, Virginia University, Blacksburg, VA 24061.*

Received December 3, 2008; Revised Manuscript Received June 8, 2009

ABSTRACT: Water penetration into thin sulfonated polyphenylene (sPP) ionomer films was investigated as a function of time, ionic strength, and film thickness by neutron reflectometry (NR). Understanding the role interfacial effects have on transport across ionic membranes is critical to the design of new responsive thin layers for a variety of applications from fuel cell membranes to protective cloths and water purification. At steady state, a nonuniform distribution of water molecules was observed with a high concentration at the air−polymer interface. An excess of water was also found at the polymer−silicon interface. The mass uptake is initially linear with $t^{0.5}$ but crosses over to an anomalous process with extended exposure periods. A delay time for the onset of diffusion is observed and is interpreted in terms of interfacial barrier to diffusion.

1. Introduction

Ionomer films have been used in numerous applications such as sensors, coatings, separation membranes, and fuel cells, in which polymer molecules form an interface with different solvents. The diffusion characteristics of the solvents in these polymeric films often define their performance.[1−7] Overall, water diffusion is remarkably sensitive to the chemical composition and the molecular weight of polymers and their structures.

Transport of solvent molecules within ionomers is a highly convoluted process that is correlated with the aforementioned physical properties of the ionomers. It is also strongly affected by temperature, the chemical nature of the solvents, and solvent-induced structural modifications, which in turn alters the physical properties of the ionomer. Numerous models have been formulated to describe this complex process.[8−12] A wide variety of techniques have been employed to measure the diffusion rates of various penetrates into polymers in order to achieve control of the process. Among these, the quartz crystal microbalance gravimetric technique and X-ray reflectivity have been used to study the moisture absorption kinetics in polyelectrolyte multilayer films as a function of film thickness.[13] Pulsed field gradient nuclear magnetic resonance (PFG-NMR) spectroscopy has been used to detect the translational motion of small molecules in polymers.[14−16] Attenuated total reflectance Fourier transform infrared (ATR-FTIR) has been used to probe solvent concentration changes within the polymer film and to obtain the diffusion rates.[17] Further insight into concentration variations as a function of time within a polymer electrolyte have been obtained by radioactive tracing.[18]

Many of these studies have depicted a time lag at the onset of solvent penetration into the films, which was interpreted as interfacial effects. While bulk diffusion studies also concluded that interfacial effects are significant, their associations with the onset of diffusion, the distribution of solvents within the matrix, and the relationship to the morphological changes that accompany the diffusion process are yet to be resolved. These effects must be accounted for in order to define boundary conditions for models used to describe multidimensional molecule transport within a polymer. In this study, we have examined water diffusion within thin ionomer films using neutron reflectometry (NR), which can probe buried interfaces, in order to elucidate the role of the interfaces.

NR has been used to the study interfacial effects in thin polymer films.[19−22] This technique resolves interfacial changes of the order of ∼1 nm, using the inherent contrast for neutrons between protonated and deuterated chains, revealing compositional changes normal to a surface.[23−26] NR is used to accurately determine not only the thickness of a film but also the shape and changes in the interfacial densities. In-situ studies of the content of the solvent as a function of z, the distance from the interface, provides a description of diffusion, averaged over the time of the measurements.[19,20,22]

The current study follows the changes that take place as small molecules diffuse into complex thin polymeric films that consist of hydrophilic−ionic groups and hydrophobic regions. Sulfonated polyphenylene (sPP) ionomers that consist of a highly rigid hydrophobic backbone with sulfonation groups substituting the lateral phenyl rings as shown in Figure 1 have been investigated at the interface with water. These ionomers were developed as ion exchange membranes with potential electrochemical and sensing applications, whereas controlling the water transport affects their utilization. The structure of thin films of polymer that consist of incompatible components such as hydrophilic and hydrophobic groups is determined by a conjunction of interfacial forces and internal phase separation of the mutually phobic groups. The degree of phase segregation and its corresponding morphology will define the diffusion pathways and will, therefore, control the rates of liquids penetration.[24,27] In order to focus on interfacial effects, the study will concentrate on thin films less that 60 nm. This thickness is comparable with several radii of gyration of the

*Corresponding author. E-mail: dperahi@ces.clemson.edu.

Published on Web 07/07/2009

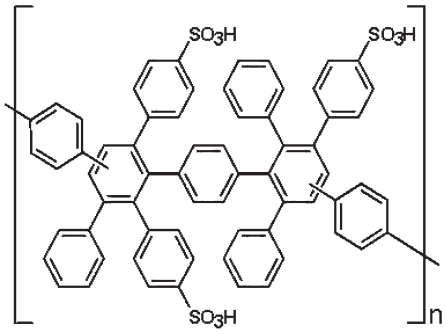

Figure 1. Chemical formula of the randomly sulfonated polyphenylene (sPP) ionomer.

polymer, where interfacial forces would affect the structure of the film. In this thickness range interfacial effects are expected to control the structure and dynamics of the polymers.

2. Experimental Section

2.1. Materials. The parent polyphenylene was polymerized using a 1:1 molar ratio of 1,4-bis(2,4,5-triphenylcyclopendienone)benzene and 1,4-diethynylbenzene in diphenyl ether at 180 °C. Polyphenylene was sulfonated using chlorosulfonic acid,[28] resulting in randomly sulfonated ionomers. The ion exchange capacity (IEC), the sulfonation levels, and the densities of the polymers are given in the Table 1.

D_2O (99.9%) was purchased from Cambridge Isotope Laboratories. The polymer films were spin-cast on a one-side-polished 75 mm wide and 5 mm thick Si wafers (Virginia Semiconductor Inc.). Dimethylformamide (DMF) (99.9%) was obtained from Aldrich Advancing Science.

2.2. Thin Film Preparation. Ionomers with IECs varying from 0.98 to 2.2 were dissolved in DMF and spin-coated on oxidized silicon wafers. The wafers were immersed in a 70:30 by volume solution of sulfuric acid and hydrogen peroxide at 82 °C for an hour. The surface-treated silicon wafers were then rinsed thoroughly with deionized water and blown dry with N_2. Film thickness was controlled by changing the solution concentration of the sPP.

2.3. Neutron Reflection Experiment. Neutron reflectivity measurements were performed on the surface profile analysis reflectometer (SPEAR) at the Lujan Neutron Scattering Center at Los Alamos National Laboratory. SPEAR is a time-of-flight reflectometer mounted on a polychromatic pulsed neutron source with a range of neutron wavelengths from 2 to 16 Å. Specular reflectivity patterns, the reflectivity normal to the surface of the polymer film, were obtained as a function of the momentum transfer vector, q, where $q = 4\pi \sin\theta/\lambda$. λ is the neutron wavelength, and θ is the incident angle. For kinetic measurements a nominal data acquisition time of 10 min was used covering a q range of 0.008−0.15 $Å^{-1}$. The statistically significant reflectivity value of measured on SPEAR is $\sim 10^{-6}$. The raw data were reduced and normalized to the incident neutron beam intensity providing reflectivity $R = I/I_0$. The error bars on the NR profiles represent the statistical errors of the measurements.

Elastic scattering detects only the amplitude of the scattered wave and not its wavelength; therefore, the density profiles obtained from elastic reflectivity are model-dependent guided either by theory or by insight from additional experiments. A multilayer recursive Parratt formalism was used to analyze the data,[29] simulating reflectivity profiles and adjusting the parameters using genetic optimization to obtain the best least-squares fit. Acceptable fits were defined as those matching the experimental results with $R^2 \geq 0.96$. The values for the scattering length densities (SLDs) were bound by the calculated values of bulk melt of the polymer and the unconfined solvent.

Table 1. IECs, Sulfonation Degrees, and Densities of sPP Studied

	IEC[a] (mmol/g)	sulfonation degree (%)	density (g/cm^3)
sPP1	0.98	13.5	1.174
sPP2	1.60	20.0	1.254
sPP4	2.20	33.3	1.360

[a] IEC = ion exchange capacity.

A consistent evolution of these parameters with film thickness and humidity was required. Specifically, the profiles were generated using a multilayer model where each layer is described as a box with a given thickness and scattering length density. The roughness between two adjacent layers was described by an error function centered at the interface. MOTOFIT, a fitting analysis package, running in IGOR was used to fit the reflectivity data.[30] The experimental error cannot be propagated through the modeling of the system to the profiles. The signal-to-noise ratio as represented by the error bars on the data and the quality of the fitting represented by R^2 define the error in the system.

Saturated conditions were defined as 100% relative humidity at 25 °C. The saturated environment is achieved by placing access of D_2O in a groove below the sample level in a sealed container that encapsulates the solvent and the sample. The activity of saturated vapor is identical to that of the liquid, since at equilibrium the chemical potentials of the liquid and the gas equal each other; therefore, the driving forces for penetration of vapor and liquids are the same. Contact with vapor offers a means to follow the onset of the interaction of the water at the interface with the polymer.

3. Results and Discussion

Films of sPP4 with different initial thicknesses from 131 to 567 Å with 33.3% sulfonation spun-cast from varying concentrations were exposed to D_2O vapors, and the kinetics was observed by subsequent measurements of reflectivity in time-averaged 10 min intervals. As previously discussed, 10 min measurements allowed collection over a sufficient range in q with good statistics.

Initial NR pattern of dry films were collected in order to establish a baseline for any subsequent changes in reflectivity as the ionomers films were exposed to saturated D_2O vapor. Figure 2a introduces representative neutron reflectivity patterns of a dry film and at various hydration stages following exposure to D_2O vapor. The experimental data marked by symbols are accompanied by fitting to a three-layer model. The pattern of the dry film is characterized by a well-defined critical edge, at q_c (critical momentum transfer, the momentum transfer corresponding to the angle below which total reflection takes place), and Kiessig fringes, resulting from the interference of the two major interfaces of the film, substrate, and air/solvent.

The film thickness, 218 Å, is determined by $2\pi/\Delta q$, where Δq is the distance between two successive minima and is further validated by the full fitting. A three-layer model was used to describe the bulk polymer and two additional layers one at the air and one at substrate interfaces. This rather clear critical edge for the dry film is a consequence of a well-defined interface with sufficient contrast between the polymer and the air. Small compositional changes as a result of D_2O absorption affect the critical angle. These changes as emphasized in the plot of the reflectivity patterns in the form of $R(q)q^4$ vs q, shown in Figure 2b, where $R(q)$ corresponds to the intensity of the reflectivity as a function as q. This form of presentation compensates for the sharp decrease arising from Fresnel reflectivity, where the intensity decays as $R(1) \propto Q_z^{-4}$,[31] resolving the features that arise from the compositional changes. As hydration takes place, the first minimum is shifted to a lower q value, and Δq between successive minima slightly decreases as a result of swelling perpendicular to the plane of the film. Furthermore, the critical

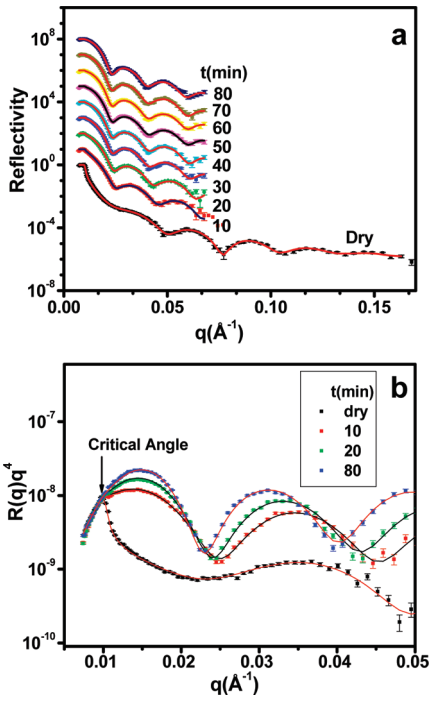

Figure 2. (a) Neutron reflectivity patterns of a thin film of sPP with 33.3% sulfonation, dry, and at the indicated exposure times to D_2O vapor. The symbols correspond to the experimental values and the lines to the results of the best fitting model. The curves are shifted vertically for clarity. (b) The low q range of $R(q)q^4$ vs q at the indicated exposure times.

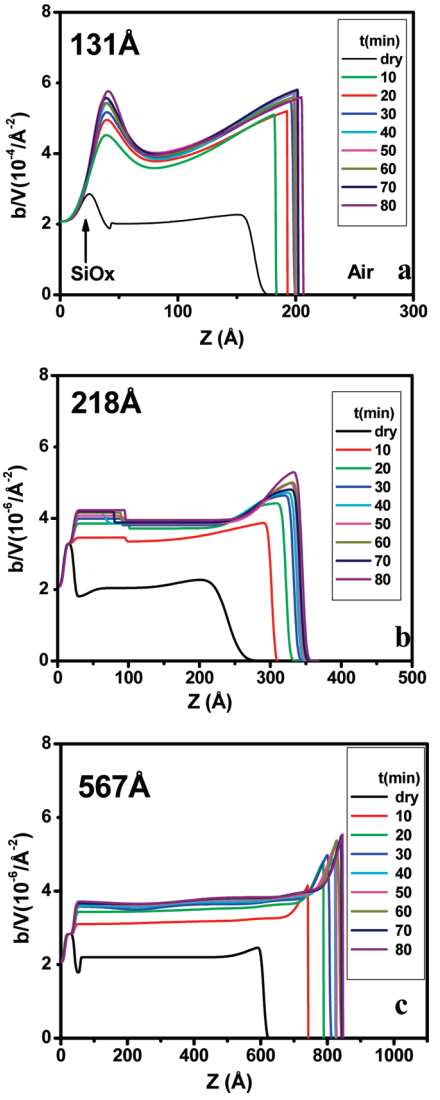

Figure 3. SLD profiles of sPPs in terms of b the scattering length and V the molar volume, derived from the reflectivity data for three films with different initial thicknesses: (a) 131, (b) 218, and (c) 567 Å, shown as a function of exposure time to D_2O vapor. Z is the distance in angstroms from the bulk silicon. The Si wafer is at $Z = 0$.

angle became less define, as seen in Figure 2b, resulting from the accumulation of D_2O at the interface or, in other words, the wetting of the polymer. At the initial stages of exposure to D_2O, q_c is lower than that of pure of D_2O ($q_c = 0.0089$ Å^{-1}); however, it is significantly higher than that of a dry polymer film. While significant changes have been observed in the critical angle, the overall film thickness is hardly affected at this early stage. These changes in the value and the sharpness of q_c provide a clear mark of the formation of a thin solvent-rich layer at the interface. The formation of such a surface layer has been further supported by significant reduction in roughness at the interface of the polymer with the vapor phase. The formation of a wetting layer is consistent with our observation that both water and toluene instantaneously and do not form a well-defined contact angle. This is surprising since the air interface is often hydrophobic predominantly due to the segregation of the lower surface tension component to the air interface to achieve the lowest energy configuration, as has been observed for fluorinated ionomers.[32,33] The dual nature of the interface with coexisting hydrophilic and hydrophobic charters is attributed to the rigidity of the backbone, which does not allow sufficient folding to bury the ionic groups. For the first time, the current study distinguishes a defined wetting layer of solvent while diffusion of water into ionic polymer membranes takes place. This is attributed to the structured nature of the interface, where because of the rigidity of the backbone, significant numbers of hydrophilic groups reside at the interface.

In order to discern the effects of the solid and air interfaces, three different thicknesses, 131, 218, and 567 Å, were investigated. The scattering length density profiles derived from the three-layer model are presented in Figure 3. The profiles for all of the dry films are characterized by a layer with slightly higher SLD at the air interface, a homogeneous intermediate layer, and a small depletion region at the film/SiO_x interface. The air interfaces are smooth with a roughness less than 10 Å. The center of the SLD profiles of the dry polymer is found to be identical to the calculated value for the bulk polymer 2.0×10^{-6} Å^{-2}, using the polymer chemical formula and the density of 1.36 g/cm^3. A depletion region the interface with solid support has been observed for several macromolecules and has been ascribed to the lower anchoring chain density.[20,33] This is a result of kinetically trapped chains at the interface that do not rearrange to the bulk density due to the reduction of orientational freedom as the solvent evaporates. An increase in density at the air interface has been predicated theoretically.[34] The model predicts that the region next to the free (air) interface becomes polymer rich due to solvent evaporation. This issue was further discussed by deGenne[35] and was observed by simulations of Tsige and Grest.[36]

As seen for all three films, both the thickness and the SLD of the hydrated films increased substantially relative to those of the dry films due to the absorption of D_2O. A D_2O-rich layer at the air interface resulted in significantly higher SLD than that of the bulk polymer layer. The amount of water accumulated in this layer increased with contact time. An excess of water has been also observed at the hydrophilic silicon oxide substrate, which decreased with increasing film thickness.

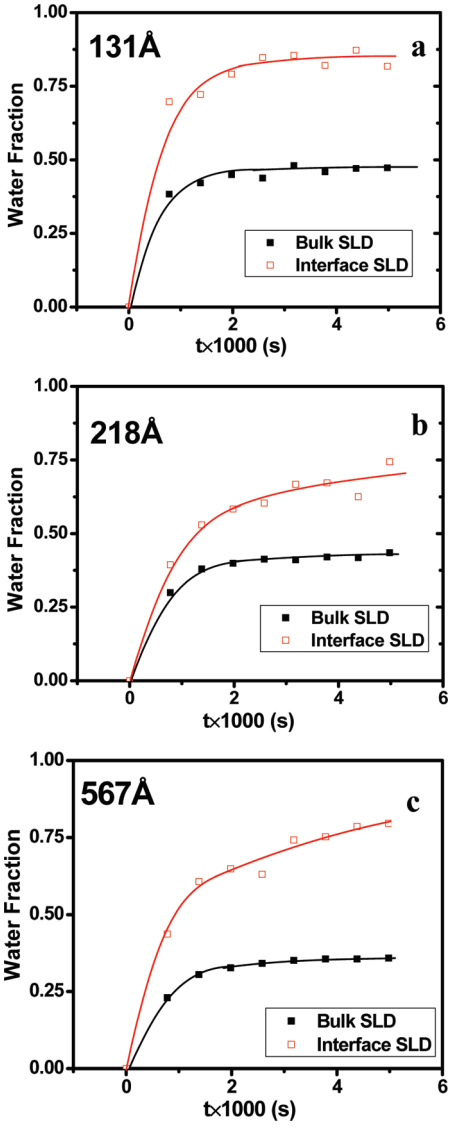

Figure 4. D_2O volume fraction of the bulk polymer layer (solid squares) measured in the center of the film, where the center is defined as half the distance to the middle point between the solid substrate and the air interface, and at the maximum SLD (open squares) at the polymer−air interface, as a function of exposure time, at the indicated initial film thicknesses.

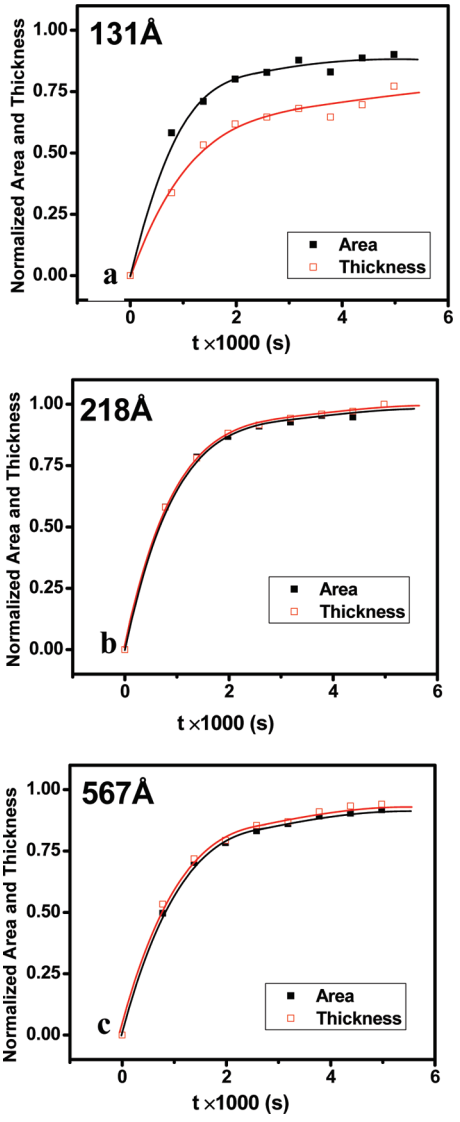

Figure 5. Changes in the total area (solid squares) and overall thickness (open squares) as a function of exposure time for films with the indicated initial thicknesses, normalized to the initial film thickness. The solid lines are a guide to the eye.

The time dependence of the changes that take place was further investigated, following the changes in the profiles as the films were exposed to the vapor. Figure 4 introduces the volume fraction of D_2O as a function of time at the maximum SLD of the air interfacial layers and at the center of the film which is defined herein as the bulk region. The volume fractions φ_{D_2O} of D_2O in the center of the films and at the air interface were determined for each film using $\rho_{tot} = \phi_{D_2O}\rho_{D_2O} + (1 - \phi_{D_2O})\rho_{polymer}$ for each film. These values show that the water levels at the air interface (~78%) are similar for all the three films after a long exposure time. However, the volume fraction of water at the center of the film decreases from 49% to 36% with increasing the initial film thickness from 131 to 567 Å. No excess water was observed at the polymer/SiO_x interface for the thick film. Repetitive experiments did not reveal any solvent accumulation at the solid interface. This difference in the behavior of thin and thick films is attributed to variations in the polymer structure and density at the solid interface as the film thickness increases. This assertion is supported by preliminary X-ray observations were in the packing of the chain as well as their correlation vary slightly as a function of film thickness.

The diffusion process affects the thickness of the film, which is the distance from the solid surface to the air interface, and the total water uptake, calculated from the integrated area of the SLD versus distance from the solid oxide surface to the air. The solid oxide surface is taken as center of the broadening function that defines the roughness of the substrate as obtained from the fitting. The air interface is defined as the center of the function that defined the roughness at the polymer−air boundary. These parameters, normalized to the thickness and total area of the SLD curves of the dry films, are plotted as a function of exposure time to D_2O vapor in Figure 5. A fast rise in the film thicknesses and areas under the curve is observed at the initial stage followed by a steady state.

The solvent uptake as a function of time as extracted from the integrated area under the SLD curves is not linear with the degree of swelling normal to the interface. In thicker films, the percentage of swelling is higher in comparison with that of thinner ones. The relation of the total amount of solvent absorbed by the polymer and the degree of swelling normal to the interface is yet another expression of interfacial effects. Interstitial space or

vacancies within the polymer film are enhanced by the presence of the interfaces, as discussed before, allowing penetration of solvent molecules without changing the total volume. Swelling does take place as these vacancies are occupied. These types of vacancies have been observed by positron annihilation and have been offered as a potential pathway for percolation of solvents in ionomer networks.[37] In thin films, the absorbed water molecules occupy free spaces in the film, thus contributing more to the increase of the SLD than to swelling on the time scale of the experiment, whereas in thick films, the polymer could more easily rearrange and swell.

It has to be noted that the films are confined to the interface, and the degree of confinement changes with film thickness. The films do not dewet as solvent penetrates, and as a result swelling takes place perpendicular to the film surface, in contrast to bulk polymers where dimensions may change in all dimensions. We will refer to the changes in dimensions normal to the interface as constrained swelling.

The mass uptake of the sPP films changes with time for all polymers and film thicknesses studied. The diffusivity of solvents into any material can be universally described by t^{α}, where t is time and where $\alpha = 0.5$ is consistent with a diffusive (Fickian) process that is accompanied by a Gaussian front. Other processes involve a flat progressing front where $\alpha = 1$. When α deviates from these values, solvent penetration involves constrained process or hopping between sites.[37,38] In the current study, within the time range required to collect the data, the solvent has penetrated across the polymer layer and reached the solid surface. While the front could not be detected, the process of solvent uptake continues for a prolonged period. The mass uptake of solvent by the thin films scaled with film thickness was plotted as a function of $t^{0.5}$ as shown in Figure 6a for three film thicknesses. A fast increase that appears linear is detected at early stages of the uptake followed by a crossover to a slower process. Zooming into the early time region, we were able to measure the penetration of solvent as early as the first 3 min, for intermediate film thicknesses. The data are shown in Figure 6b, where a clear crossover from a linear dependence of the uptake with $t^{0.5}$ is observed for two different sulfonation levels, indicative of a diffusive process. Interestingly though, the extrapolation of the uptake does not intercept the time axis at $t = 0$ but at later time, suggestive of an interfacial barrier to solvent penetration. Both films with significantly different IECs exhibit an initial similar behavior at early exposure times.

From the linear range of the mass uptake with $t^{0.5}$, we have calculated the diffusivity at the onset of penetration

$$M_t/M_\infty = (2/T)(Dt/\pi)^{1/2}$$

where M_t is the equilibrium mass uptake at time t, M_∞ is the maximum mass uptake at infinite time, D is the diffusivity of the guest molecules, and T is the film thickness. This model assumes that the penetrant propagate on is one-dimensional, which is valid given the large surface area-to-volume ratio and the impermeable substrate. Diffusivity of the order of magnitude of 10^{-15} cm^2/s is obtained for these films. The diffusivities extracted from these data are given in Table 2. There is no clear correlation between film thickness and the diffusivity. These values are comparable with those of water diffusion in other ultrathin polymer films[19−21,38] which have been found to be several orders of magnitude slower than in free-standing membranes. Diffusivity as calculated from NMR for Nafion is on the order of 10^{-6}−10^{-7} cm^2/s,[39−41] and recent diffusion measurements from mass transport provide values of 10^{-8} cm^2/s.[42]

With this value of diffusivity, within the time frame of 10−20 min, before a crossover from diffusive to anomalous behavior is observed, the solvent would have propagated only 10−20 Å, depending of the specific film, which is inconsistent with the fact that within 3 min water is distributed across the film. These values however are consistent with a surface barrier that, once overcome, the water spreads throughout the film. A close inspection of the polymer patterns derived from the reflectometry shows that the dry film consists of a higher density film or "crusting" at the interface,[34−36] which results in a barrier that the solvent has to cross. While the polymer may rearrange with time, the air interface remains different than the center of the film throughout the time frame of our measurements.

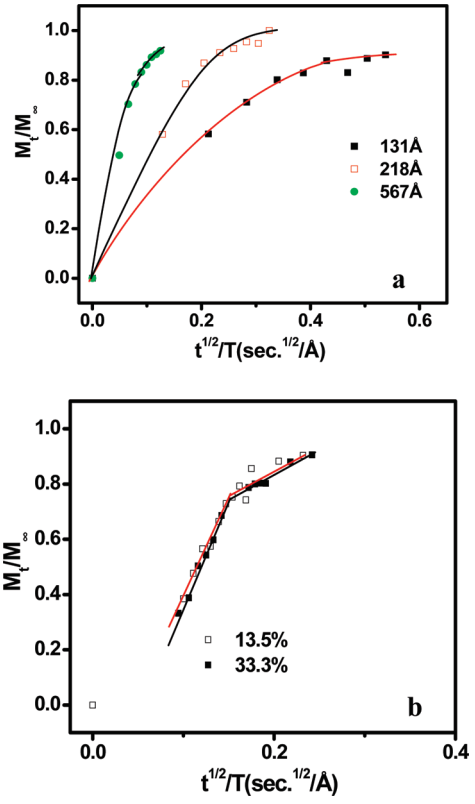

Figure 6. Water uptake as a function of $t^{0.5}$, scaled by film thickness for (a) films with different initial thicknesses and (b) films with different IEC. The symbols represent the experimental data, and the lines are a guide to the eye.

Table 2. Swelling Degrees and Diffusion Coefficients of sPP4 with Different Thicknesses

initial thickness (Å)	constrained swelling (%)	$D \times 10^{-15}$ (cm^2/s)
131	40	0.24
217	48	1.16
567	44	5.43

Transport studies[42] carried out in micrometer thick membranes have shown that permeation has been inversely proportional to the membrane thickness when the membranes were in direct contact with liquid water. In contact with vapor, however, 10-fold slower diffusion rates were detected attributed to interfacial effects.

The initial mass uptake for thicker films is faster than in thinner films, which is consistent with previous reports.[19,20] It may be either a direct the result of morphological changes due to the variation in film thickness or a result of competition between interfacial effects and elasticity of the films. The morphological factors that would contribute include polymer chain ordering, chain orientation, intermolecular packing density, and the presence of microvoids which have been observed in bulk ionomers.

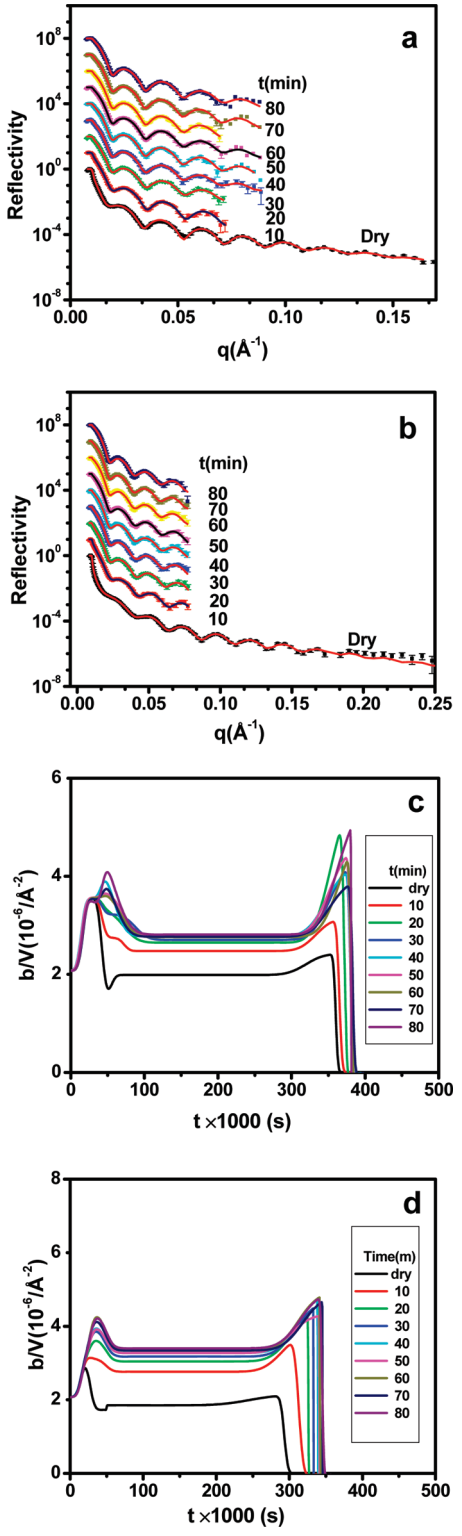

Figure 7. Neutron reflectivity patterns (symbols) and their fitting (lines) of dry and hydrated sPP1 and sPP2 films exposed to D_2O (sulfonation levels: 13.5% and 20%, respectively). In (a) and (b), the curves are shifted vertically for a clearer view. The corresponding polymer profiles are plotted in (c) and (d).

In bulk films, polymer chains are randomly oriented, while in thin films either higher or lower degree of polymer chain orientation occurs due to interfacial interactions. Increased order in a thin film reduces the polymer chain mobility, triggering a drop in the overall diffusion of penetrants within that material. With increasing film thickness, the interfacial confinement decreases, resulting in a higher degree of freedom of the polymer chain. Consequently, thicker films have a higher water molecule capacity and thus greater diffusion rates.

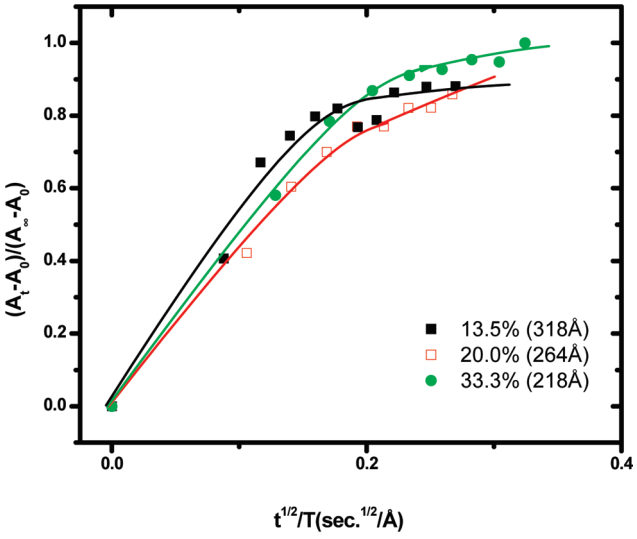

Figure 8. Water uptake as a function of $t^{0.5}$ scaled by film thickness for samples with different sulfonation levels as indicated, normalized to the initial film thickness.

Table 3. Swelling Degrees of sPP Membranes with Different IECs

IEC (mmol/g)	constrained swelling (%)
0.98	11
1.60	25
2.20	48

The behavior at long exposure time is attributed to chains relaxation resulting from swelling stress that allows an increased amount of water to imbue the film. As water molecules penetrate, the network expands and the polymer chains are less confined. As a result, the overall ionomers network becomes more dynamic, which in turn allows further water permeation.

The increase of film thickness, or constrained swelling, as a result of solvent uptake as a function of the initial dry width is listed in Table 2. The films exhibit significantly different expansion degrees despite having the same ionic content. The dependence of the constrained swelling on the ion content was investigated as a function of IEC for two sPP films (1.6 and 0.98 mmol/g). With the experimental challenge of obtaining identical film thicknesses, 264 and 318 Å films were studied. The reflectivity patterns and corresponding SLD profiles are shown in Figure 7 . Figure 8 describes the normalized water uptake as a function of $t^{0.5}$ as extracted from the area under the SLD curves.

In comparison, the film thicknesses at equilibrium for these samples are 323, 330, and 354 Å. The degree of constrained swelling for these samples was 11%, 25%, and 48%, as listed in Table 3. The maximum amount of absorbed water is proportional to the ion content. Qualitatively, the degree of swelling at extended exposure times to D_2O vapor varies with the degree of sulfonation; however, no quantitative correlations could be extracted. The degree of swelling and the diffusivity at the onset of solvent penetration are strongly affected by the interfacial effects on the structure of the polymer.

4. Summary

Penetration of D_2O into thin polymer films of sPP is affected by interfacial forces including the polymer interactions with the solid support and the air interface, resulting in a nonuniform distribution of the water in the film. A thin D_2O-rich layer

accumulated at the air interface, which is consistent with wetting of the interface. As the solvent diffused into the layers, swelling perpendicular to the plane of the film takes place. This directional swelling results from confinement effects. The uptake of water however was found to be larger than the increase in volume for thin films. Excess of D_2O has been also observed at the solid interface in thin films, where its extent depends on film thickness. At early exposure times, the mass uptake of D_2O scales with $t^{0.5}$ and diverges at a later stage. The diffusivity at the early stages of exposure to water vapors was found to be significantly slower than the bulk transport, attributed to the interfacial effects. In summary, the solvent penetration into thin films of rigid ionic polymers is dominated by interfacial effects at both the air and solid boundaries.

Acknowledgment. We thank DOE for partial funding support under Contract DE-FG02-07ER46456.T Sandia National Laboratories is a multiprogram laboratory operated by Sandia Corporation, a Lockheed Martin Company, for the United States Department of Energy's National Nuclear Security Administration is acknowledged for support under DE-AC04-94AL85000. This work was supported by Los Alamos National Laboratory and Lujan Center under DOE Contract W7405-ENG-36, the DOE Office of Basic Energy Science.

Supporting Information Available: Reflectometry patterns as a function of exposure time to water vapor and the corresponding SLD profiles (Figure 1s); reflectometry patterns and the corresponding fitting for different film thickness (Figure 2s). This material is available free of charge via the Internet at http://pubs.acs.org.

References and Notes

(1) Pineri, M.; Eisenberg, A. *Structure and Properties of Ionomers*; D. Reidel Publishing Co.: Dordrecht, Holland, 1987.
(2) Schlick, S. *Ionomers: Characterization, Theory and Applications*; CRC Press: Boca Raton, FL, 1996.
(3) Truffler-Boutry, D.; Geyer, A. D.; Diat, O.; Gebel, G. *Macromolecules* **2007**, *40*, 8259.
(4) Ugo, P.; Moretto, L. M.; Vezzà, F. *ChemPhysChem* **2002**, *3*, 917.
(5) Maki, N.; Tajitsu, Y.; Sasaki, H. *Packag. Technol. Sci.* **2007**, *20*, 309.
(6) Van del Wel, G. K.; Adan, O. C. G. *Prog. Org. Coat.* **1999**, *37*, 1.
(7) Paddison, S. J. *J. New Mater. Electrochem. Syst.* **2001**, *4*, 207.
(8) Sanopoulou, M.; Petropoulos, J. H. *Macromolecules* **2001**, *34*, 1400.
(9) Lin, H.; Steyerl, A.; Satija, S. K.; Karim, A.; Russell, T. P. *Macromolecules* **1995**, *28*, 1470.
(10) Yi, X.; Pellegrino, J. *J. Polym. Sci., Part B: Polym. Phys* **2002**, *40*, 980.
(11) Aucejo, S.; Marco, C.; GavaRa, R. *J. Appl. Polym. Sci.* **1999**, *74*, 1201.
(12) Mcknight, H. S.; Gillespie, W. J. *J. Appl. Polym. Sci.* **1997**, *64*, 1971.
(13) Vogt, B. D.; Soles, C. L.; Lee, H.; Lin, E. K.; Wu, W.-L. *Langmuir* **2004**, *20*, 1453.
(14) Wang, Y.; Meresi, G.; Gosselin, J.; Azar, D.; Wen, W-Y.; Jones, A. A.; Inglefield, P. T. *Macromolecules* **2001**, *34*, 6680.
(15) Kriz, J. *Langmuir* **2004**, *20*, 9560.
(16) Zhang, J.; Giotto, M. V.; Wen, W. Y.; Jones, A. A. *J. Membr. Sci.* **2006**, *269*, 118.
(17) Hallinan, D. T.; Elabd, Y. A. *J. Phys. Chem. B* **2007**, *111*, 13221.
(18) Stolwijk, N. A.; Obeidi, S. *Phys. Rev. Lett.* **2004**, *93*, 125901.
(19) Vogt, B. D.; Prabhu, V. M.; Soles, C. L.; Jones; Satija, S. K.; Lin, E. K.; Wu, W.-L. *Langmuir* **2005**, *21*, 2460.
(20) Mukherjee, M.; Singh, A.; Daillant, J.; Menelle, A.; Cousin, F. *Macromolecules* **2007**, *40*, 1073.
(21) Vogt, B. D.; Soles, C. L.; Jones, R. L.; Wang, C.-Y.; Lin, E. K.; Wu, W.-L.; Satija, K. S. *Langmuir* **2004**, *20*, 5285.
(22) Tanchak, M. O.; Yager, G. K.; Fritzsche, H.; Harroun, T.; Katsaras, J.; Barrett, C. *Langmuir* **2006**, *22*, 5137.
(23) Higgins, J. S.; Benoit, H. C. *Polymer and Neutron Scattering*, Oxford University Press: New York, 1996; p 342.
(24) Shin, K.; Raifailovich, M. H.; Sokolov, J.; Gersappe, D. *Langmuir* **2001**, *17*, 6675.
(25) Bucknall, G. D.; Higgins, S. J.; Butler, A. S. *J. Polym. Sci., Part B: Polym. Phys.* **2004**, *42*, 3267.
(26) Russell, T. P. *Mater. Sci. Rep.* **1990**, *5*, 171.
(27) Elliot, J. A.; Hanna, S.; Elliot, A. M. S. *Polymer* **2001**, *42*, 2251.
(28) Fujimoto, C. H.; Hickner, M. A.; Cornelius, C. J.; Loy, D. A. *Macromolecules* **2005**, *38*, 5010.
(29) Paratt, L. G. *Phys. Rev. Lett.* **1954**, *95*, 359.
(30) Nelson, A. *J. Appl. Crystallogr.* **2006**, *39*, 273.
(31) Alsnielsen, J. *Physica A* **1986**, *140*, 376.
(32) Gottesfeld, S.; Zawodzinski, Jr., T. A.; Alkire, R. C. et al. *Advances in Electrochemical Science and Engineering*; Wiley-VCH: New York, 1997; Vol. *5*, p 195.
(33) Zawodzinski, T. A.Jr.; Gottesfeld, S.; Shoichet, S.; McCarthy, T. J. *J. Appl. Electrochem.* **1993**, *23*, 86.
(34) Bornside, D. E.; Macosko, C. W.; Scriven, L. E. *J. Appl. Phys.* **1989**, *66*, 5135.
(35) Reiter, G.; De Gennes, P. G. *Eur. Phys. J. E* **2001**, *6*, 25.
(36) Tsige; Mesfin; Mattsson; Thomas, R.; Grest; Gary, S. *Macromolecules* **2004**, *37*, 9132.
(37) Crank, J. *The Mathematics of Diffusion*, 2nd ed.; Clarendon: Oxford, 1975.
(38) Edmondson, C. A.; Fontanella, J. J. *Solid State Ionics* **2002**, *152−153*, 355.
(39) He, L.; Fujimoto, C. H.; Cornelius, C. J.; Perahia, D. Confined water behaviors in rigid ionic membranes, manuscript in preparation.
(40) Ohkubo, T.; Kidena, K.; Ohira, A. *Macromolecules* **2008**, *41*, 8688.
(41) Nicotera, I.; Khalfan, A.; Goenaga, G.; Zhang, T.; Bocarsly, A.; Greenbaum, S. *Ionics* **2008**, *14*, 243.
(42) Majsztrik, P.; Bocarsly, A.; Benziger, J. *J. Phys. Chem. B* **2008**, *112*, 16280.